Article

Heterometallic Europium(III)–Lutetium(III) Terephthalates as Bright Luminescent Antenna MOFs

Viktor G. Nosov [1], Arkady S. Kupryakov [1], Ilya E. Kolesnikov [1], Aleksandra A. Vidyakina [1], Ilya I. Tumkin [1], Stefaniia S. Kolesnik [1], Mikhail N. Ryazantsev [1,2], Nikita A. Bogachev [1], Mikhail Yu. Skripkin [1] and Andrey S. Mereshchenko [1,*]

1   Saint-Petersburg State University, 7/9 Universitetskaya emb., 199034 St. Petersburg, Russia
2   Nanotechnology Research and Education Centre RAS, Saint Petersburg Academic University, ul. Khlopina 8/3, 194021 St. Petersburg, Russia
*   Correspondence: a.mereshchenko@spbu.ru; Tel.: +7-951-677-5465

Abstract: A new series of luminescent heterometallic europium(III)–lutetium(III) terephthalate metal–organic frameworks, namely $(Eu_xLu_{1-x})_2bdc_3 \cdot nH_2O$, was synthesized using a direct reaction in a water solution. At the Eu^{3+} concentration of 1–40 at %, the MOFs were formed as a binary mixture of the $(Eu_xLu_{1-x})_2bdc_3$ and $(Eu_xLu_{1-x})_2bdc_3 \cdot 4H_2O$ crystalline phases, where the $Ln_2bdc_3 \cdot 4H_2O$ crystalline phase was enriched by europium(III) ions. At an Eu^{3+} concentration of more than 40 at %, only one crystalline phase was formed: $(Eu_xLu_{1-x})_2bdc_3 \cdot 4H_2O$. All MOFs containing Eu^{3+} exhibited sensitization of bright Eu^{3+}-centered luminescence upon the 280 nm excitation into a $^1\pi\pi^*$ excited state of the terephthalate ion. The fine structure of the emission spectra of Eu^{3+} $^5D_0$-^7F_J (J = 0–4) significantly depended on the Eu^{3+} concentration. The luminescence quantum yield of Eu^{3+} was significantly larger for Eu-Lu terephthalates containing a low concentration of Eu^{3+} due to the absence of Eu-Eu energy migration and the presence of the Ln_2bdc_3 crystalline phase with a significantly smaller nonradiative decay rate compared to the $Ln_2bdc_3 \cdot 4H_2O$.

Keywords: metal–organic framework; luminescence; rare earth; europium; lutetium; phase transition

1. Introduction

In recent decades, rare-earth-element metal–organic frameworks (REE-MOFs) were actively designed and synthetized due to their unique luminescence properties. They are unique platforms for fabricating advanced luminescent materials, which are widely used in various fields of science and technology [1–4]. The position of the lanthanide ionic luminescence bands strongly depends only on the lanthanide ion, which allows the construction of REE-MOFs with the desired optical properties [5]. Taking this fact into account and considering the high stability, low solubility and toxicity, and highly effective charge transport of Ln-MOFs, they are prospective materials for OLEDs [6,7], luminescent thermometers [8,9], and imaging [10–13]. Variations in organic linkers in MOFs allow synthetic chemists to form structures with different porosities large surface areas, and high structural flexibility [14–16], which allows the use of REE-MOFs as highly selective sensors on organic and inorganic materials [17–25]. Typical linkers in REE-MOFs are organic carboxylates due to the simple synthesis of REE-MOFs in undemanding conditions and the unlimited possibilities in MOF design [26,27].

Lanthanide ions possess characteristic luminescence; however, direct UV excitation of them is inefficient because they have very small light absorption coefficients: 4f-4f transitions are forbidden by selection rules. This issue can be resolved using the energy transfer from the excited linker to the lanthanide ion (antenna effect) [28,29]. Aromatic organic molecules such as 1,4-benzenedicarboxylate (bdc) are widely used as antenna linkers due to their effective UV absorbance and pronounced antenna effect [30,31]. Usually,

the energy transfer takes place from the lower-level triplet electronic state (T_1) of the linker molecule but not from the lowest excited singlet state (S_1). In some cases, the heavy lanthanides increase the rate of S_1-T_1 intersystem crossing [32–35]. The high concentration of luminescent lanthanide ion in homometallic REE-MOFs could result in concentration quenching through Ln-Ln energy migration and, therefore, the drop in luminescence quantum yield (PLQY) [36]. Utochnikova et al. proposed a solution to this problem by doping of a luminescent europium(III) terephthalate with nonluminescent Gd^{3+} ions, which not only diluted the luminescent Tb^{3+} ions, but also increased the probability of intersystem crossing, which increased the PLQY. It was found that Eu-Gd and Eu-Y heterometallic terephthalates were formed in the same crystalline phases. In the current work, we studied a series of luminescent heterometallic europium(III)–lutetium(III) terephthalates MOFs and observed that the substitution of a large amount of Eu(III) for Lu(III) resulted in a crystalline phase change as well as a significant rise in the PLQY.

2. Results and Discussion

2.1. XRD Results and Analysis

The X-ray powder diffraction (XRD) patterns (Figure 1a) were measured for the range of heterometallic europium(III)–lutetium(III) terephthalates (Eu_xLu_{1-x})$_2$bdc$_3$·nH$_2$O; bdc = 1,4-benzenedicarboxylate) with a Eu^{3+} concentration from 0 to 100 at %. An analysis of the XRD patterns demonstrated that in a range of Eu^{3+} concentration of 6 to 100 at %, the samples were isostructural to the Ln$_2$bdc$_3$·4H$_2$O (Ln = Ce-Yb) [37]. This structure, which is common for the rare-earth terephthalates from Ce to Yb [38], was a three-dimensional metal–organic framework (MOF) in which octacoordinated lanthanide ions were bound to the two water molecules and six terephthalate ions through the oxygen atoms (Figure 1b). The analysis of XRD patterns of Eu-Lu terephthalates with 0–2 at % of Eu^{3+} showed that the samples were isostructural to Er$_2$bdc$_3$ [38], which is a 3D MOF in which heptacoordinated lanthanide ions are bound to the seven oxygen atoms from the terephthalate ions (Figure 1c). At a Eu^{3+} concentration in the range of 3–5 at %, both the Ln$_2$bdc$_3$·4H$_2$O and Ln$_2$bdc$_3$ crystalline phases were observed. The XRD peaks for heterometallic europium(III)–lutetium(III) terephthalates in Eu^{3+} concentration ranged from 6 to 100 at % and were slightly shifted relative to the XRD peaks measured for Ln$_2$bdc$_3$·4H$_2$O reported previously [37]. To compare these Ln$_2$bdc$_3$·4H$_2$O structures, the refinement of unit cell parameters was performed for some samples with a Eu^{3+} concentration between 6 and 100 at % (Table 1) using UnitCell software [39], which retrieved unit cell parameters from diffraction data using a method of least squares from the 2Θ data of the XRD patterns. Calculation errors also are shown in Table 1. We observed that in the range, the unit cell parameters increased. The observed growth of the unit cell parameters of heterometallic europium(III)–lutetium(III) terephthalates was explained by the smaller ionic radius of the octacoordinated Lu^{3+} (0.977 Å) compared with the ionic radius of the Eu^{3+} ion (1.066 Å) [40].

Table 1. Unit cell parameters with calculation errors for (Eu_xLu_{1-x})$_2$bdc$_3$·nH$_2$O refined for Eu$_2$bdc$_3$·4H$_2$O crystalline phase.

χ_{Eu} (%)	a, Å	b, Å	c, Å	α	β	γ	V, Å^3
100	6.1904 ±0.0019	9.856 ±0.003	10.251 ±0.003	101.673 ±0.027	90.273 ±0.028	104.796 ±0.025	591.13 ±0.22
90	6.1862 ±0.0019	9.845 ±0.003	10.236 ±0.003	101.583 ±0.027	90.300 ±0.028	104.727 ±0.025	589.63 ±0.22
60	6.1727 ±0.0018	9.815 ±0.003	10.206 ±0.003	101.553 ±0.027	90.418 ±0.028	104.657 ±0.025	585.00 ±0.22
40	6.1635 ±0.0018	9.783 ±0.003	10.179 ±0.003	101.497 ±0.027	90.472 ±0.028	104.651 ±0.025	580.75 ±0.22
20	6.1405 ±0.0018	9.738 ±0.003	10.145 ±0.003	101.570 ±0.027	90.562 ±0.028	104.617 ±0.025	573.90 ±0.21

Table 1. *Cont.*

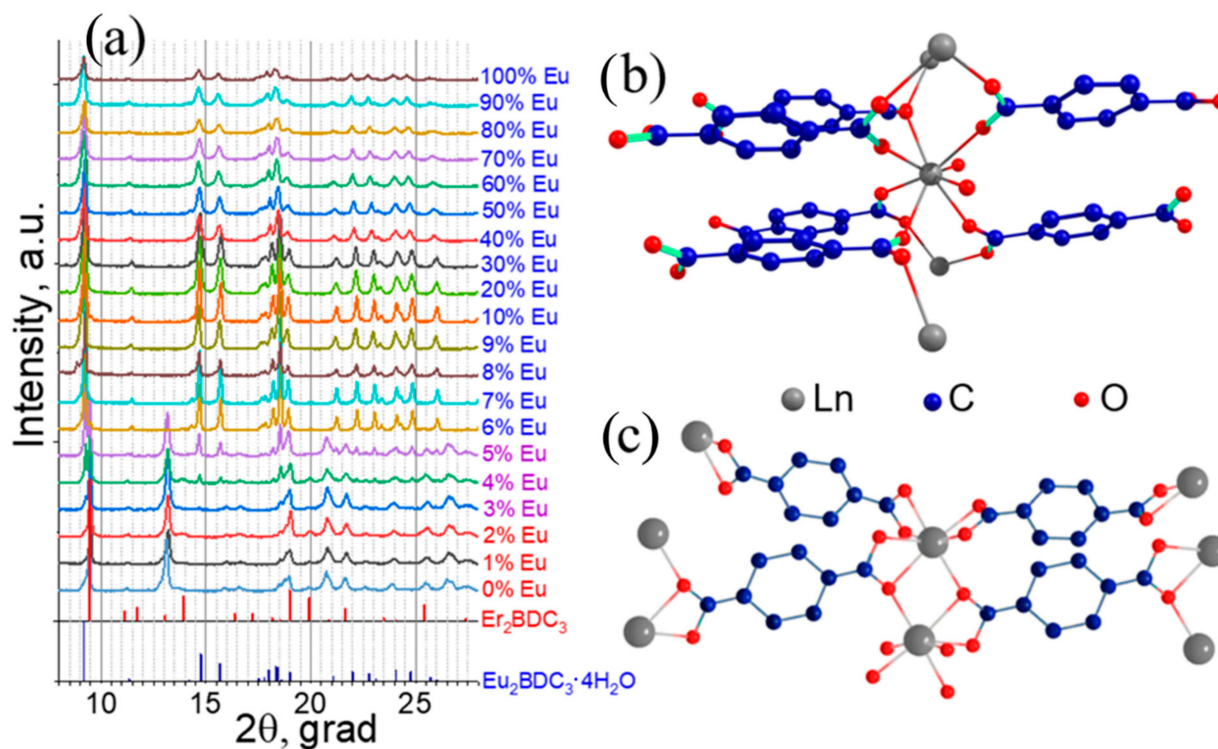| χ_{Eu} (%)	a, Å	b, Å	c, Å	α	β	γ	V, Å^3
10	6.1411 ±0.0018	9.7178 ±0.003	10.1334 ±0.003	101.626 ±0.026	90.461 ±0.028	104.590 ±0.025	572.13 ±0.21
6	6.1313 ±0.0018	9.714 ±0.003	10.130 ±0.003	101.582 ±0.026	90.474 ±0.027	104.608 ±0.025	570.784 ±0.21

Figure 1. (**a**) The XRD patterns of $(Eu_xLu_{1-x})_2bdc_3 \cdot nH_2O$ in heterometallic europium(III)–lutetium(III) terephthalate powders from 0% Eu^{3+} to 100% Eu^{3+}) and the simulated XRD pattern of Er_2bdc_3 and $Eu_2bdc_3 \cdot 4H_2O$ single-crystals structure taken from refs. [37,38]. (**b**,**c**) The generated crystal structures of $Eu_2bdc_3 \cdot 4H_2O$ and Er_2bdc_3, respectively.

2.2. Thermogravimetric Analysis (TGA)

The thermogravimetric analysis (TGA) was carried out for the selected heterometallic europium(III)–lutetium(III) terephthalates in a temperature range of 25–300 °C (Figure 2a). The mass loss was observed at 120–180 °C for all measured samples. As previously reported [38], the mass loss in this temperature range can be assigned to the dehydration of the compounds resulting in the formation of Ln_2bdc_3. An analysis of the TGA curves allowed us to calculate the average numbers of water molecules in the heterometallic europium(III)–lutetium(III) terephthalates ($(Eu_xLu_{1-x})_2bdc_3 \cdot nH_2O$). We observed that this number increased with the increase in the Eu^{3+} concentration (Figure 2b). An analysis of the XRD patterns demonstrated the presence of two crystalline phases: $Ln_2bdc_3 \cdot 4H_2O$ and Ln_2bdc_3. Therefore, we could estimate the molar fraction of each coexisting crystalline phase (Figure 2c). The molar fraction of $Ln_2bdc_3 \cdot 4H_2O$ increased along with the Eu^{3+} concentration in a range between 0 and 40 at %. In the Eu^{3+} concentration range of 40–100%, only $Ln_2bdc_3 \cdot 4H_2O$ was present.

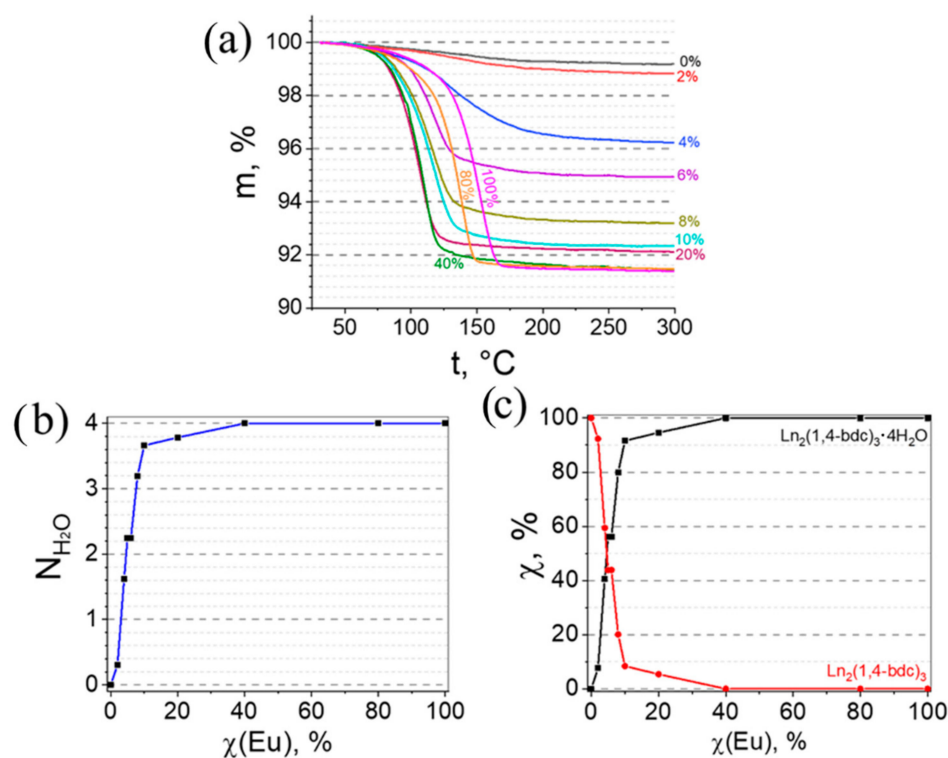**Figure 2.** (**a**) Thermogravimetric analysis (TGA) curves showing the mass loss profile of $(Eu_xLu_{1-x})_2$ $bdc_3 \cdot xH_2O$ during thermal decomposition; (**b**) the number of water molecules per one formula unit in $(Eu_xLu_{1-x})_2bdc_3 \cdot xH_2O$; (**c**) the molar fraction of Ln_2bdc_3 and $Ln_2bdc_3 \cdot 4H_2O$ in heterometallic europium(III)–lutetium(III) terephthalates as a function of Eu concentration.

2.3. Luminescent Properties

The terephthalate ion is a typical linker used in luminescent antenna MOFs [41] due to its intensive UV absorbance [42] followed by efficient energy transfer to the luminescent lanthanide ion. The excitation of $(Eu_xLu_{1-x})_2bdc_3 \cdot nH_2O$ ($\lambda_{ex.}$ = 280 nm) resulted in emission in the visible range corresponding to $^5D_0$-^7F_J (J = 0–5) transitions of the Eu^{3+} ion [5] (Figures 3 and 4). Upon UV excitation, the terephthalate ion was promoted into the $S_n(^1\pi\pi^*)$ state followed by the fast internal conversion to $S_1(^1\pi\pi^*)$. Due to the heavy atom effect, the S_1 state efficiently moved to the $T_1(^3\pi\pi^*)$ triplet electronic excited state [34] via intersystem crossing. The T_1 state of the terephthalate ion [34] ($\approx$20,000 cm^{-1}) had a higher energy than the $^5D_1$ energy level of the Eu^{3+} ion [5] ($\approx$19,000 cm^{-1}) and a significantly lower energy than that of the lower excited state of the Lu^{3+} ion [43] (80,000 cm^{-1}). Therefore, an efficient energy transfer from the T_1 triplet electronic excited state of the terephthalate ion to the $^5D_1$ energy level of the Eu^{3+} ion occurred. The $^5D_1$ level of the Eu^{3+} ion then underwent an internal conversion into the $^5D_0$ energy level followed by the emission into the ^7F_J (J = 0–4) lower-lying levels.

We observed that the fine structure of the Eu^{3+} emission spectra significantly depended on the Eu^{3+} concentration in the $(Eu_xLu_{1-x})_2bdc_3 \cdot nH_2O$ (Figure 4). At Eu^{3+} ion concentrations of more than 6 at %, in which the $Ln_2bdc_3 \cdot 4H_2O$ phase dominated, the emission spectra were similar to that of $Eu_2bdc_3 \cdot 4H_2O$ [31] and consisted of narrow bands corresponding to $^5D_0$-^7F_J (J = 0–4) transitions of Eu^{3+}: $^5D_0$-$^7F_0$ (577.6 nm), $^5D_0$-$^7F_1$ (587.9 and 591.5 nm), $^5D_0$-$^7F_2$ (614.0 nm), $^5D_0$-$^7F_3$ (649.0 nm), and $^5D_0$-$^7F_4$ (697.0 nm) (Figure 3). At low Eu^{3+} concentrations (2 and 4 at % Eu^{3+}), in which the Ln_2bdc_3 phase dominated, the fine structure of the emission spectra was significantly different. The emission spectra contained $^5D_0$-$^7F_0$ (577.2 nm and 577.6 nm), $^5D_0$-$^7F_1$ (585.9, 588.4, and 595.6 nm), $^5D_0$-$^7F_2$ (606.6, 610.2, 616.6, 619.4 (shoulder), and 621.8 nm), $^5D_0$-$^7F_3$ (649.0 nm), and $^5D_0$-$^7F_4$ (700.0 nm) Eu^{3+} narrow emission bands.

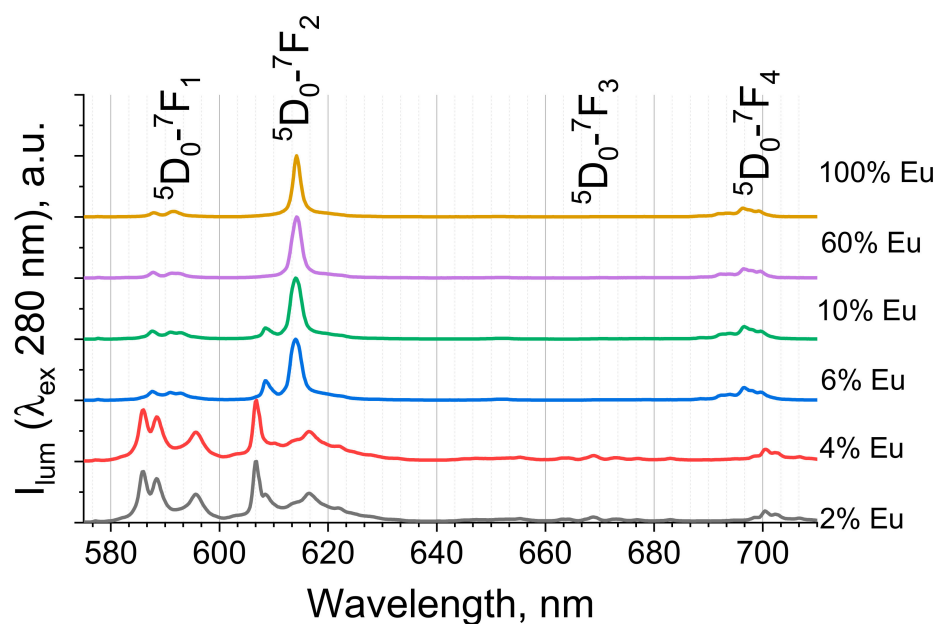**Figure 3.** The normalized emission spectra of $(Eu_xLu_{1-x})_2bdc_3 \cdot nH_2O$ at selected Eu^{3+} concentrations (given in legend) upon 280 nm excitation.
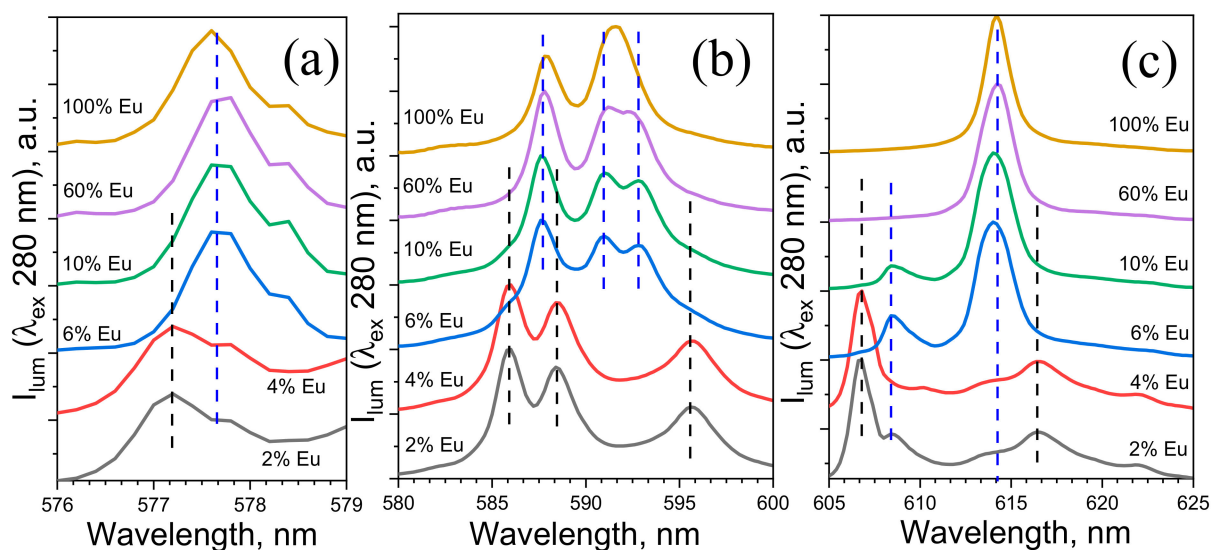

Figure 4. Fine structure of lines in emission spectra of heterometallic europium(III)–lutetium(III) terephthalates normalized at maximum point for (**a**) $^5D_0$-$^7F_0$, (**b**) $^5D_0$-$^7F_1$, and (**c**) $^5D_0$-$^7F_2$ transitions.

$^5D_0$-$^7F_0$ transition is strictly forbidden by the Judd–Ofelt theory; one can observe this transition only for europium(III) ions in coordination sites with C_n, C_{nv}, and C_s symmetry. For all measured samples, $^5D_0$-$^7F_0$ transitions were observed. The analysis of the fine structure of this transition allowed us to determine the number of Eu^{3+} coordination sites because the $^7F_0$ level was not degenerate and did not split in the crystal field, hence $^5D_0$-$^7F_0$ could present in the emission spectrum as a single line for one type of Eu^{3+} coordination. The fine structure of the $(Eu_xLu_{1-x})_2bdc_3 \cdot nH_2O$ emission bands $^5D_0$-$^7F_0$ is shown in Figure 4a. In the emission spectra of Eu-Lu terephthalates with a Eu^{3+} concentration of 6–100 at %, a single line was observed in the 570–585 nm range ($^5D_0$-$^7F_0$) with a maximum at 577.6 nm, which indicated that Eu^{3+} ions existed in the single-crystal-phase isostructural $Ln_2bdc_3 \cdot 4H_2O$. Meanwhile, by using a TGA, we estimated the molar fractions of $Ln_2bdc_3 \cdot 4H_2O$ and Ln_2bdc_3 as equal to 60 and 40%, respectively. Therefore, the single $^5D_0$-$^7F_0$ emission band (6–100 at % Eu^{3+}) can be explained by uneven ion distribution

between the two phases: the $Ln_2bdc_3 \cdot 4H_2O$ crystalline phase was enriched by Eu^{3+} ions. In the Eu-Lu terephthalates with 2–4 at % Eu^{3+}, two emission bands corresponding to the $^5D_0$-$^7F_0$ transition were observed to peak at 577.2 and 577.6 nm, indicating the two different coordination sites of the Eu^{3+} ion. Therefore, in the terephthalates containing 2–4 at % Eu^{3+}, europium(III) ions were distributed between two phases, namely $Ln_2bdc_3 \cdot 4H_2O$ and Ln_2bdc_3, which was consistent with the TGA and XRD data.

The fine structure of the $^5D_0$-^7F_J emission bands and their relative intensities were very sensitive to the Eu^{3+} ions' local symmetry. The degeneracy of each spin–orbit level was 2J+1 [5]. Hence, the maximum amount of crystal-field transitions of the $^5D_0$-$^7F_1$ and $^5D_0$-$^7F_2$ transitions were 3 and 5, respectively. According to previous studies, lanthanide(III) ions had pseudo-C_4 symmetry in $Ln_2bdc_3 \cdot 4H_2O$ (Ln = Tb, Eu) [38]. For $Eu_2bdc_3 \cdot 4H_2O$ (100 at % Eu^{3+}), the $^5D_0$-$^7F_1$ transition split into two crystal field transitions (587.9 and 591.6 nm), and the $^5D_0$-$^7F_2$ transition was presented in the emission spectrum as a single line (614.0 nm). Interestingly, for the Eu-Lu terephthalates containing 6–60 at % Eu^{3+}, different splitting patterns of the $^5D_0$-^7F_J transitions in the crystal field were observed. The $^5D_0$-$^7F_1$ and $^5D_0$-$^7F_2$ transition split into three (587.6, 591.0, and 592.8 nm) and two components (608.5 and 614.0 nm), respectively (Figure 4b,c). The difference between the abovementioned emission spectra can be explained by the distortion of the coordination polyhedron due to the appearance of structural defects caused by the addition of Lu^{3+} ions, which have a lower ionic radius than europium(III) ions (lanthanide contraction). This resulted in the lowering of the local symmetry of the Eu^{3+} ion and the larger number of crystal-field transitions of Eu-Lu terephthalates compared to the $Eu_2bdc_3 \cdot 4H_2O$. The number of $^5D_0$-^7F_J crystal-field transitions indicated that the Eu^{3+} had symmetry of C_2 or lower [44].

In the emission spectra of Ln_2bdc_3 (2–4 at % Eu^{3+}), the $^5D_0$-$^7F_1$ and $^5D_0$-$^7F_2$ transitions split into three (585.9, 588.4, and 595.6 nm) and five components (606.6, 610.2, 616.6, 619.4 (shoulder), and 621.8 nm), respectively. In the emission spectra of the Lu-Eu terephthalates containing 2–4 at % Eu^{3+}, we observed the presence of $(Eu_xLu_{1-x})_2bdc_3 \cdot 4H_2O$ emission bands (weak 608.5 and 614.0 nm signals) because the Eu^{3+} ion was distributed between the Ln_2bdc_3 and $Ln_2bdc_3 \cdot 4H_2O$ crystalline phases. A careful analysis of the Ln_2bdc_3 crystalline structure (Figure 1c) allowed us to conclude that the Ln^{3+} ion had C_1 local symmetry, which was consistent with the number of crystal-field components of the $^5D_0$-$^7F_0$, $^5D_0$-$^7F_1$, and $^5D_0$-$^7F_2$ transitions (1, 3, and 5, respectively) [44].

The luminescence decay curves of the $(Eu_xLu_{1-x})_2bdc_3 \cdot nH_2O$ phosphors monitored at 615 nm ($^5D_0$-$^7F_2$ transition) are presented in Figure 5 ($\lambda_{ex.}$ = 280 nm). At a low Eu^{3+} concentration (2 and 4 at %), the decay curves were fitted by a double exponential function (1), whereas the decay curves of the Eu-Lu terephthalates containing 6–100 at % Eu^{3+} were fitted by a single exponential function (2):

$$I = I_1 \cdot e^{-\frac{t}{\tau_1}} + I_2 \cdot e^{-\frac{t}{\tau_2}} \tag{1}$$

$$I = I_1 \cdot e^{-\frac{t}{\tau_1}} \tag{2}$$

where τ_1 and τ_2 are the observed $^5D_0$ lifetimes (Table 2).

Table 2. The lifetimes of excitation state 5D0 of Eu^{3+} in heterometallic europium(III)–lutetium(III) terephthalates at 2, 4, 6, 10, 60, and 100 at % Eu.

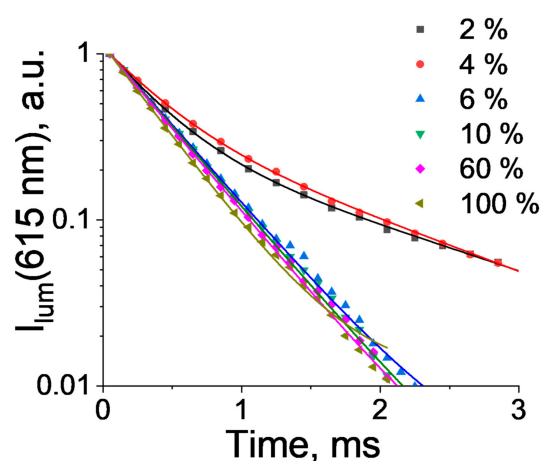| χ_{Eu} (%)	τ_1, ms	τ_2, ms	PLQY, %
100	0.390		10 ± 1
60	0.435		11 ± 1
10	0.449		12 ± 1
6	0.459		16 ± 1
4	0.392	1.602	22 ± 1
2	0.367	1.878	22 ± 1

Figure 5. The 615 nm luminescence decay curves of heterometallic europium(III)–lutetium(III) terephthalates at 2, 4, 6, 10, 60, and 100 at % Eu.

The Eu-Lu terephthalates containing 6–100 at % Eu^{3+} had $^5D_0$ lifetimes of 0.390–0.459 ms and luminescence quantum yields of 10–16%. The measured PLQY of the $Eu_2bdc_3 \cdot 4H_2O$ was comparable with the literature data [31,38,45]. The $^5D_0$ lifetime values and the luminescence quantum yields decreased with an increase in the Eu^{3+} concentration due to the energy migration between the Eu^{3+} ions and subsequent quenching by impurities and defects. We demonstrated in this work that Eu^{3+} ions predominantly existed in the $Ln_2bdc_3 \cdot 4H_2O$ phase in the europium(III)–lutetium(III) terephthalates containing 6–100 at % Eu^{3+}, in which the presence of a single Eu^{3+} coordination site resulted in a single $^5D_0$ lifetime. Interestingly, the europium(III)–lutetium(III) terephthalates containing 2–4 at % Eu^{3+} were characterized by two $^5D_0$ lifetimes. One emission decay component (τ_1 = 0.392–0.367 ms) was close to the value observed for the europium(III)–lutetium(III) terephthalates containing 6–100 at % Eu^{3+}, while another component (τ_2 = 1.602–1.878 ms) was 4–4.8 times larger. In the Eu-Lu terephthalates containing 2–4 at % Eu^{3+}, the Eu^{3+} ions were distributed between the $Ln_2bdc_3 \cdot 4H_2O$ and Ln_2bdc_3 crystalline phases. Therefore, τ_1 and τ_2 could be assigned to the Eu^{3+} ions located in the $Ln_2bdc_3 \cdot 4H_2O$ and Ln_2bdc_3, respectively. The water molecules in the $Ln_2bdc_3 \cdot 4H_2O$ structure were coordinated with the Eu^{3+} ion and quenched the Eu^{3+} luminescence due to efficient energy transfer to high-energy O-H stretching vibrational modes of coordinated water molecules [46,47]. In the Ln_2bdc_3 crystalline phase, the Eu^{3+} ion was coordinated only with oxygen atoms of carboxylic groups of terephthalate ions. The efficient quenching of Eu^{3+} ions by water molecules in the $Ln_2bdc_3 \cdot 4H_2O$ structure resulted in a significant decrease in the Eu^{3+} ion $^5D_0$ lifetime compared to anhydrous Ln_2bdc_3. The emission quantum yield of the Eu^{3+} was significantly larger for the Eu-Lu terephthalates doped with a low Eu^{3+} concentration. This observation can be explained by two reasons: the absence of efficient Eu-Eu energy migration and the presence of the Ln_2bdc_3 crystalline phase with a significantly smaller nonradiative decay rate compared to the $Ln_2bdc_3 \cdot 4H_2O$.

3. Materials and Methods

Lutetium (III) chloride hexahydrate and europium (III) chloride hexahydrate were purchased from Chemcraft (Kaliningrad, Russia). Benzene-1,4-dicarboxylic (terephthalic, H_2bdc) acid (>98%), sodium hydroxide (>99%), nickel(II) chloride hexahydrate (>99%), and EDTA disodium salt (0.1 M aqueous solution) were purchased from Sigma-Aldrich Pty Ltd. (Germany) and used without additional purification. The 0.2M solutions of $EuCl_3$ and $LuCl_3$ were prepared and standardized using complexometric titration with EDTA. A total of 0.6 mole of sodium hydroxide and 0.3 mole of terephthalic acid were dissolved in distilled water to obtain a 1 L solution of a 0.3 M solution of the disodium terephthalate (Na_2bdc).

The heterometallic europium(III)–lutetium(III) terephthalates were obtained by mixing 1 mL of 0.2 M $EuCl_3$ and $LuCl_3$ aqueous solutions taken in stoichiometric ratios with 2 mL of 0.3 M Na_2bdc water solution (Table 3). White precipitates of heterometallic europium(III)–lutetium(III) terephthalates were separated from the reaction mixture using centrifugation ($4000 \times g$) and washed using deionized water 5 times. All samples were driedat 60 °C.

Table 3. The heterometallic europium(III)–lutetium(III) terephthalates' synthesis conditions.

χ_{Eu}, %	V(0.2M $EuCl_3$), mL	V(0.2M $LuCl_3$), mL
0	0	1.00
1	0.01	0.99
2	0.02	0.98
3	0.03	0.97
4	0.04	0.96
5	0.05	0.95
6	0.06	0.94
7	0.07	0.93
8	0.08	0.92
9	0.09	0.91
10	0.10	0.90
20	0.20	0.80
30	0.30	0.70
40	0.40	0.60
50	0.50	0.50
60	0.60	0.40
70	0.70	0.30
80	0.80	0.20
90	0.90	0.10
100	1.00	0

The Eu^{3+}/Lu^{3+} ratios in the heterometallic europium(III)–lutetium(III) terephthalates were confirmed using energy-dispersive X-ray spectroscopy (EDX) (EDX spectrometer EDX-800P, Shimadzu, Japan) (Table 4). The Eu/Lu ratios measured via EDX were consistent with the ratios of Eu^{3+}/Lu^{3+} taken for the synthesis in the form of $EuCl_3$ and $LuCl_3$ aqueous solutions (Table 3). The X-ray powder diffraction (XRD) measurements were performed on a D2 Phaser (Bruker, USA) X-ray diffractometer using Cu K_α radiation ($\lambda = 1.54056$ Å). The thermogravimetry curves were obtained using a TG 209 F1 Libra thermo-microbalance (Netzsch, Germany). The luminescence spectra were recorded with a Fluoromax-4 fluorescence spectrometer (Horiba Jobin Yvon, Japan). Lifetime measurements were performed with the same spectrometer using a pulsed Xe lamp (pulse duration: 3 µs). The absolute values of the photoluminescence quantum yields were recorded using a Fluorolog 3 Quanta-phi device. All measurements were performed at 25 °C.

Table 4. Eu^{3+} atomic fraction (relative to the total amount of Eu^{3+} and Lu^{3+}) in heterometallic europium(III)–lutetium(III) terephthalates taken during synthesis and obtained from EDX data.

χ_{Eu} (%), Taken	χ_{Eu} (%), EDX
0	0
2	2.07 ± 0.21
4	3.9 ± 0.4
5	4.7 ± 0.5
6	6.3 ± 0.6
10	10.2 ± 1.0
20	19.3 ± 1.9
40	37 ± 4
80	80 ± 8
100	100

4. Conclusions

In this work, we reported on the photoluminescence properties of luminescent antenna MOF—heterometallic europium(III)–lutetium(III) terephthalates. The series of $(Eu_xLu_{1-x})_2bdc_3 \cdot nH_2O$ (x = 0–1) was synthesized in the aqueous solution. At Eu^{3+} concentrations of 1–40 at %, the heterometallic europium(III)–lutetium(III) terephthalates were formed as a mixture of the $(Eu_xLu_{1-x})_2bdc_3$ and $(Eu_xLu_{1-x})_2bdc_3 \cdot 4H_2O$ crystalline phases. At higher Eu^{3+} concentrations, a single crystalline phase was formed: $(Eu_xLu_{1-x})_2bdc_3 \cdot 4H_2O$. All the synthesized samples containing Eu^{3+} demonstrated a bright red emission corresponding to the $^5D_0$-^7F_J (J = 0–4) transitions of Eu^{3+} ions upon 280 nm excitation into the singlet electronic excited state of terephthalate ions. An analysis of the fine structure of the emission spectra allowed us to conclude that the Eu^{3+} ions were unevenly distributed between the Ln_2bdc_3 and $Ln_2bdc_3 \cdot 4H_2O$ phases: the $Ln_2bdc_3 \cdot 4H_2O$ crystalline phase was enriched by Eu^{3+} ions. The local symmetry of the Eu^{3+} ions in the heterometallic Eu-Lu terephthalates was proposed based on a careful analysis of the fine structure of the emission spectra and the structural data. We demonstrated that the $^5D_0$ excited state lifetimes were 4–4.8 times larger for Eu^{3+} in the Ln_2bdc_3 crystalline phase than in $Ln_2bdc_3 \cdot 4H_2O$ due to the absence of luminescence quenching of the Eu^{3+} by coordinated water molecules. The luminescence quantum yields of terephthalate ions decreased with an increase in the europium concentration from 2 to 100 at % Eu^{3+} ($\lambda_{ex.}$ = 280 nm).

References

1. Xia, T.; Zhang, J. Our Journey of Developing Dual-emitting Metal-organic Framework-based Fluorescent Sensors. *Z. Anorg. Allg. Chem.* **2022**, *648*, e202100355. [CrossRef]
2. Han, X.; Liu, J.; Yu, K.; Lu, Y.; Xiang, W.; Zhao, D.; He, Y. Water-Stable Eu $_6$ -Cluster-Based Fcu-MOF with Exposed Vinyl Groups for Ratiometric and Fluorescent Visual Sensing of Hydrogen Sulfide. *Inorg. Chem.* **2022**, *61*, 5067–5075. [CrossRef]
3. Zhao, D.; Yu, K.; Han, X.; He, Y.; Chen, B. Recent Progress on Porous MOFs for Process-Efficient Hydrocarbon Separation, Luminescent Sensing, and Information Encryption. *Chem. Commun.* **2022**, *58*, 747–770. [CrossRef] [PubMed]
4. Bryleva, Y.A.; Artem'ev, A.V.; Glinskaya, L.A.; Rakhmanova, M.I.; Samsonenko, D.G.; Komarov, V.Y.; Rogovoy, M.I.; Davydova, M.P. Bright Photo- and Triboluminescence of Centrosymmetric Eu(Iii) and Tb(Iii) Complexes with Phosphine Oxides Containing Azaheterocycles. *New J. Chem.* **2021**, *45*, 13869–13876. [CrossRef]
5. Binnemans, K. Interpretation of Europium(III) Spectra. *Coord. Chem. Rev.* **2015**, *295*, 1–45. [CrossRef]

6.   Kozlov, M.I.; Aslandukov, A.N.; Vashchenko, A.A.; Medvedko, A.V.; Aleksandrov, A.E.; Grzibovskis, R.; Goloveshkin, A.S.; Lepnev, L.S.; Tameev, A.R.; Vembris, A.; et al. On the Development of a New Approach to the Design of Lanthanide-Based Materials for Solution-Processed OLEDs. *Dalton Trans.* **2019**, *48*, 17298–17309. [CrossRef]

7.   Shurygin, A.V.; Vovna, V.I.; Korochentsev, V.V.; Mirochnik, A.G.; Kalinovskaya, I.V.; Sergienko, V.I. Optical Properties and Electronic Structure of Eu(III) Complexes with HMPA and TPPO. *Spectrochim. Acta A Mol. Biomol. Spectrosc.* **2021**, *250*, 119397. [CrossRef]

8.   Khudoleeva, V.; Tcelykh, L.; Kovalenko, A.; Kalyakina, A.; Goloveshkin, A.; Lepnev, L.; Utochnikova, V. Terbium-Europium Fluorides Surface Modified with Benzoate and Terephthalate Anions for Temperature Sensing: Does Sensitivity Depend on the Ligand? *J. Lumin.* **2018**, *201*, 500–508. [CrossRef]

9.   Zhou, X.; Wang, H.; Jiang, S.; Xiang, G.; Tang, X.; Luo, X.; Li, L.; Zhou, X. Multifunctional Luminescent Material Eu(III) and Tb(III) Complexes with Pyridine-3,5-Dicarboxylic Acid Linker: Crystal Structures, Tunable Emission, Energy Transfer, and Temperature Sensing. *Inorg. Chem.* **2019**, *58*, 3780–3788. [CrossRef]

10.   Liu, D.; Lu, K.; Poon, C.; Lin, W. Metal-Organic Frameworks as Sensory Materials and Imaging Agents. *Inorg. Chem.* **2014**, *53*, 1916–1924. [CrossRef]

11.   Panikar, S.S.; Ramírez-García, G.; Vallejo-Cardona, A.A.; Banu, N.; Patrón-Soberano, O.A.; Cialla-May, D.; Camacho-Villegas, T.A.; de La Rosa, E. Novel Anti-HER2 Peptide-Conjugated Theranostic Nanoliposomes Combining NaYF4:Yb,Er Nanoparticles for NIR-Activated Bioimaging and Chemo-Photodynamic Therapy against Breast Cancer. *Nanoscale* **2019**, *11*, 20598–20613. [CrossRef]

12.   Liu, H.; Lu, W.; Wang, H.; Rao, L.; Yi, Z.; Zeng, S.; Hao, J. Simultaneous Synthesis and Amine-Functionalization of Single-Phase BaYF5:Yb/Er Nanoprobe for Dual-Modal In Vivo Upconversion Fluorescence and Long-Lasting X-ray Computed Tomography Imaging. *Nanoscale* **2013**, *5*, 6023–6029. [CrossRef] [PubMed]

13.   Shen, T.; Zhang, Y.; Kirillov, A.M.; Hu, B.; Shan, C.; Liu, W.; Tang, Y. Versatile Rare-Earth Oxide Nanocomposites: Enhanced Chemo/Photothermal/Photodynamic Anticancer Therapy and Multimodal Imaging. *J. Mater. Chem. B* **2016**, *4*, 7832–7844. [CrossRef] [PubMed]

14.   Liu, W.; Yin, R.; Xu, X.; Zhang, L.; Shi, W.; Cao, X. Structural Engineering of Low-Dimensional Metal–Organic Frameworks: Synthesis, Properties, and Applications. *Adv. Sci.* **2019**, *6*, 1802373. [CrossRef] [PubMed]

15.   Ryu, U.J.; Jee, S.; Rao, P.C.; Shin, J.; Ko, C.; Yoon, M.; Park, K.S.; Choi, K.M. Recent Advances in Process Engineering and Upcoming Applications of Metal–Organic Frameworks. *Coord. Chem. Rev.* **2021**, *426*, 213544. [CrossRef] [PubMed]

16.   Cook, T.R.; Zheng, Y.R.; Stang, P.J. Metal-Organic Frameworks and Self-Assembled Supramolecular Coordination Complexes: Comparing and Contrasting the Design, Synthesis, and Functionality of Metal-Organic Materials. *Chem. Rev.* **2013**, *113*, 734–777. [CrossRef] [PubMed]

17.   Puglisi, R.; Pellegrino, A.L.; Fiorenza, R.; Scirè, S.; Malandrino, G. A Facile One-Pot Approach to the Synthesis of Gd-Eu Based Metal-Organic Frameworks and Applications to Sensing of Fe^{3+} and $Cr_2O_7^{2-}$ Ions. *Sensors* **2021**, *21*, 1679. [CrossRef]

18.   Lustig, W.P.; Mukherjee, S.; Rudd, N.D.; Desai, A.V.; Li, J.; Ghosh, S.K. Metal-Organic Frameworks: Functional Luminescent and Photonic Materials for Sensing Applications. *Chem. Soc. Rev.* **2017**, *46*, 3242–3285. [CrossRef]

19.   Liu, D.; Dong, G.; Wang, X.; Nie, F.; Li, X. A Luminescent Eu Coordination Polymer with Near-Visible Excitation for Sensing and Its Homologues Constructed from 1,4-Benzenedicarboxylate and 1: H-Imidazo[4,5-f] [1,10]-Phenanthroline. *CrystEngComm* **2020**, *22*, 7877–7887. [CrossRef]

20.   Ding, S.B.; Wang, W.; Qiu, L.G.; Yuan, Y.P.; Peng, F.M.; Jiang, X.; Xie, A.J.; Shen, Y.H.; Zhu, J.F. Surfactant-Assisted Synthesis of Lanthanide Metal-Organic Framework Nanorods and Their Fluorescence Sensing of Nitroaromatic Explosives. *Mater. Lett.* **2011**, *65*, 1385–1387. [CrossRef]

21.   Zhao, J.J.; Liu, P.Y.; Dong, Z.P.; Liu, Z.L.; Wang, Y.Q. Eu(III)-Organic Framework as a Multi-Responsive Photoluminescence Sensor for Efficient Detection of 1-Naphthol, Fe^{3+} and MnO_4^{4-} in Water. *Inorg. Chim. Acta* **2020**, *511*, 119843. [CrossRef]

22.   Han, X.; Gu, C.; Ding, Y.; Yu, J.; Li, K.; Zhao, D.; Chen, B. Stable Eu^{3+}/Cu^{2+}-Functionalized Supramolecular Zinc(II) Complexes as Fluorescent Probes for Turn-On and Ratiometric Detection of Hydrogen Sulfide. *ACS Appl. Mater. Interfaces* **2021**, *13*, 20371–20379. [CrossRef] [PubMed]

23.   Dong, C.L.; Li, M.F.; Yang, T.; Feng, L.; Ai, Y.W.; Ning, Z.L.; Liu, M.J.; Lai, X.; Gao, D.J. Controllable Synthesis of Tb-Based Metal–Organic Frameworks as an Efficient Fluorescent Sensor for Cu^{2+} Detection. *Rare Met.* **2021**, *40*, 505–512. [CrossRef]

24.   Nguyen, L.H.; Oveissi, F.; Chandrawati, R.; Dehghani, F.; Naficy, S. Naked-Eye Detection of Ethylene Using Thiol-Functionalized Polydiacetylene-Based Flexible Sensors. *ACS Sens.* **2020**, *5*, 1921–1928. [CrossRef]

25.   Feng, L.; Dong, C.; Li, M.; Li, L.; Jiang, X.; Gao, R.; Wang, R.; Zhang, L.; Ning, Z.; Gao, D.; et al. Terbium-Based Metal-Organic Frameworks: Highly Selective and Fast Respond Sensor for Styrene Detection and Construction of Molecular Logic Gate. *J. Hazard. Mater.* **2020**, *388*, 121816. [CrossRef]

26.   Janicki, R.; Mondry, A.; Starynowicz, P. Carboxylates of Rare Earth Elements. *Coord. Chem. Rev.* **2017**, *340*, 98–133. [CrossRef]

27.   Utochnikova, V.V.; Kuzmina, N.P. Photoluminescence of Lanthanide Aromatic Carboxylates. *Russ. J. Coord. Chem.* **2016**, *42*, 679–694. [CrossRef]

28.   Cao, W.; Tang, Y.; Cui, Y.; Qian, G. Energy Transfer in Metal–Organic Frameworks and Its Applications. *Small Struct.* **2020**, *1*, 2000019. [CrossRef]

29.   Yin, H.Q.; Wang, X.Y.; Yin, X.B. Rotation Restricted Emission and Antenna Effect in Single Metal-Organic Frameworks. *J. Am. Chem. Soc.* **2019**, *141*, 15166–15173. [CrossRef]

30. Do Nascimento, J.F.S.; Barros, B.S.; Kulesza, J.; de Oliveira, J.B.L.; Pereira Leite, A.K.; de Oliveira, R.S. Influence of Synthesis Time on the Microstructure and Photophysical Properties of Gd-MOFs Doped with Eu^{3+}. *Mater. Chem. Phys.* **2017**, *190*, 166–174. [CrossRef]

31. Kolesnik, S.S.; Nosov, V.G.; Kolesnikov, I.E.; Khairullina, E.M.; Tumkin, I.I.; Vidyakina, A.A.; Sysoeva, A.A.; Ryazantsev, M.N.; Panov, M.S.; Khripun, V.D.; et al. Ultrasound-Assisted Synthesis of Luminescent Micro-and Nanocrystalline Eu-Based Mofs as Luminescent Probes for Heavy Metal Ions. *Nanomaterials* **2021**, *11*, 2448. [CrossRef] [PubMed]

32. Okuno, Y.; Cavagnero, S. Effect of Heavy Atoms on Photochemically Induced Dynamic Nuclear Polarization in Liquids. *J. Magn. Reson.* **2018**, *286*, 172–187. [CrossRef] [PubMed]

33. Cui, G.; Fang, W.H. State-Specific Heavy-Atom Effect on Intersystem Crossing Processes in 2-Thiothymine: A Potential Photodynamic Therapy Photosensitizer. *J. Chem. Phys.* **2013**, *138*, 044315. [CrossRef]

34. Utochnikova, V.V.; Grishko, A.Y.; Koshelev, D.S.; Averin, A.A.; Lepnev, L.S.; Kuzmina, N.P. Lanthanide Heterometallic Terephthalates: Concentration Quenching and the Principles of the "Multiphotonic Emission". *Opt. Mater.* **2017**, *74*, 201–208. [CrossRef]

35. Bryleva, Y.A.; Ustimenko, Y.P.; Plyusnin, V.F.; Mikheilis, A.V.; Shubin, A.A.; Glinskaya, L.A.; Komarov, V.Y.; Agafontsev, A.M.; Tkachev, A.V. Ln(Iii) Complexes with a Chiral 1H-Pyrazolo[3,4-b]Pyridine Derivative Fused with a (−)-α-Pinene Moiety: Synthesis, Crystal Structure, and Photophysical Studies in Solution and in the Solid State. *New J. Chem.* **2021**, *45*, 2276–2284. [CrossRef]

36. Kolesnikov, I.E.; Vidyakina, A.A.; Vasileva, M.S.; Nosov, V.G.; Bogachev, N.A.; Sosnovsky, V.B.; Skripkin, M.Y.; Tumkin, I.I.; Lähderanta, E.; Mereshchenko, A.S. The Effect of Eu^{3+} and Gd^{3+} co-Doping on the Morphology and Luminescence of NaYF4:Eu^{3+}, Gd^{3+} phosphors. *New J. Chem.* **2021**, *45*, 10599–10607. [CrossRef]

37. Reineke, T.M.; Eddaoudi, M.; Fehr, M.; Kelley, D.; Yaghi, O.M. From Condensed Lanthanide Coordination Solids to Microporous Frameworks Having Accessible Metal Sites. *J. Am. Chem. Soc.* **1999**, *121*, 1651–1657. [CrossRef]

38. Daiguebonne, C.; Kerbellec, N.; Guillou, O.; Bünzli, J.C.; Gumy, F.; Catala, L.; Mallah, T.; Audebrand, N.; Gérault, Y.; Bernot, K.; et al. Structural and Luminescent Properties of Micro- and Nanosized Particles of Lanthanide Terephthalate Coordination Polymers. *Inorg. Chem.* **2008**, *47*, 3700–3708. [CrossRef]

39. Holland, T.J.B.; Redfern, S.A.T. Unit Cell Refinement from Powder Diffraction Data: The Use of Regression Diagnostics. *Mineral. Mag.* **1997**, *61*, 65–77. [CrossRef]

40. Shannon, R.D. Revised Effective Ionic Radii and Systematic Studies of Interatomie Distances in Halides and Chaleogenides. *Acta Crystallogr. Sect. A* **1976**, *32*, 751–767. [CrossRef]

41. Cui, Y.; Yue, Y.; Qian, G.; Chen, B. Luminescent Functional Metal-Organic Frameworks. *Chem. Rev.* **2012**, *112*, 1126–1162. [CrossRef] [PubMed]

42. Alammar, T.; Hlova, I.Z.; Gupta, S.; Biswas, A.; Ma, T.; Zhou, L.; Balema, V.; Pecharsky, V.K.; Mudring, A.V. Mechanochemical Synthesis, Luminescent and Magnetic Properties of Lanthanide Benzene-1,4-Dicarboxylate Coordination Polymers (Ln0.5Gd0.5)2 (1,4-BDC)3(H_2O)4; Ln = Sm, Eu, Tb. *New J. Chem.* **2020**, *44*, 1054–1062. [CrossRef]

43. Dieke, G.H.; Crosswhite, H.M. The Spectra of the Doubly and Triply Ionized Rare Earths. *Appl. Opt.* **1963**, *2*, 675–686. [CrossRef]

44. Tanner, P.A. Some Misconceptions Concerning the Electronic Spectra of Tri-Positive Europium and Cerium. *Chem. Soc. Rev.* **2013**, *42*, 5090–5101. [CrossRef] [PubMed]

45. Haquin, V.; Etienne, M.; Daiguebonne, C.; Freslon, S.; Calvez, G.; Bernot, K.; le Pollès, L.; Ashbrook, S.E.; Mitchell, M.R.; Bünzli, J.C.; et al. Color and Brightness Tuning in Heteronuclear Lanthanide Terephthalate Coordination Polymers. *Eur. J. Inorg. Chem.* **2013**, *2013*, 3464–3476. [CrossRef]

46. Li, M.; Zhou, Y.; Yao, Y.; Gao, T.; Yan, P.; Li, H. Designing Water-Quenching Resistant Highly Luminescent Europium Complexes by Regulating the Orthogonal Arrangement of Bis-β-Diketone Ligands. *Dalton Trans.* **2021**, *50*, 9914–9922. [CrossRef]

47. Ivanova, A.A.; Gontcharenko, V.E.; Lunev, A.M.; Sidoruk, A.V.; Arkhipov, I.A.; Taydakov, I.V.; Belousov, Y.A. New Carboxylate Anionic Sm-MOF: Synthesis, Structure and Effect of the Isomorphic Substitution of Sm^{3+} with Gd^{3+} and Tb^{3+} Ions on the Luminescent Properties. *Inorganics* **2022**, *10*, 104. [CrossRef]